Investigating Aerodynamic Performance of Vertical Axis Wind Turbines Using Computational Techniques

Muhammad Ahmad [1*], Iram Rehman [2]

[1] Department of Aerospace Engineering, College of Aeronautical Engineering, National University of Sciences and Technology, Islamabad, Pakistan

[2] Bahauddin Zakariya University, Multan, Pakistan

*** Corresponding author:*** Muhammad Ahmad, muhammad.ahmad@cae.nust.edu.pk

Abstract: This paper presents a comprehensive aerodynamic analysis of H-Rotor Darrieus and Savonius turbines utilizing advanced computational fluid dynamics (CFD) techniques. H-Rotor Darrieus turbines, characterized by fixed blades, often encounter challenges with self-starting, while Savonius turbines exhibit good starting capabilities albeit with lower power coefficients (C_p). In this study, the sliding mesh technique was employed to investigate the intricate flow fields over the airfoil geometry, H-Rotor Darrieus turbine, and Savonius turbine. The analysis revealed that Savonius turbine starts generating power at a low wind speed of 2 m/s, while the H-Rotor Darrieus requires a slightly higher wind speed of 3.1 m/s to begin operation. Moreover, the maximum rated power of the H-Rotor Darrieus turbine was found to be 30 watts, which was significantly higher than the Savonius turbine's maximum rated power of 5 watts. The C_p for H-Rotor Darrieus and Savonius turbines were meticulously determined across a range of tip speed ratios (TSRs), with remarkable peak values of 0.32 and 0.21 achieved at TSRs of 1.69 and 0.75, respectively. The comparison of CFD results with experimental data revealed that the H-Rotor Darrieus configuration consistently outperformed its Savonius counterpart, particularly in high wind speed conditions. The results showed that the maximum absolute difference between the experimental and CFD values is 1.3 watts for the Savonius turbine and 4.5 watts for the H-Rotor Darrieus turbine. These small absolute differences indicate the accuracy and reliability of the simulations. By offering valuable insights into the design configurations, this present study establishes a foundation for achieving superior performance and efficiency in vertical axis wind turbine (VAWT). The high-fidelity analysis provided through CFD simulations proves instrumental in the early design phase, enabling engineers to make informed decisions and refine their designs with greater confidence.

Keywords: Aerodynamics; CFD analysis; H-Rotor Darrieus; Savonius turbine and VAWT

1. INTRODUCTION

Since the establishment of the industrial system, the world's energy consumption has significantly expanded. Advances in renewable energy are more important than ever given the exponential rise in population and the strain this has placed on the limited resources. It is anticipated that fossil fuel-based energy supplies will not be enough to fulfil the demand for energy. The ecology and the availability of energy resources have both suffered greatly as a result of industrialization. Additionally, rising energy consumption is a sign of both the energy crisis and environmental problems. It is predicted that humanity would experience a scarcity of essential energy sources since the available fossil fuels on Earth have become extremely restricted and has been gradually declining over time. To stop further depletion of natural resources and mitigate catastrophic environmental deterioration, the incorporation of sustainable growth principles and the establishment of metrics for technological processes, consequences, and operational constraints are crucial [1]. According to projections in global energy technology, failure to swiftly develop alternative energy sources will result in a substantial increase in greenhouse gas emissions across various energy sectors over the coming decades. **Figure 1** illustrates the decline in carbon emissions for different energy systems. To tackle the challenges posed by emissions, a fundamental transformation in energy technology is necessary. This shift should prioritize key areas such as energy efficiency, nuclear power, renewable energy sources, and the decarbonization of fossil fuels. Researchers are currently focusing their attention on developing safe, secure, and environmentally friendly renewable energy sources [2]. There are several alternative energy generation options; some of them include solar energy, wind energy, geothermal energy, hydropower, and biomass [3]. The most promising, long-term, and viable alternative energy source now in use, with the benefits of extremely minimal environmental impact, affordable pricing, and sustainable solutions, is wind energy.

Significant attempts have been made to enhance wind energy technologies in order to fulfil the rising demand for electricity and minimize reliance on energy imports. Research has been done in several nations to pinpoint locations with the best wind speeds. The technology in the global energy industry that is now increasing at the highest rate is wind energy. By the end of 2025, the capacity for producing wind power might exceed 200,000 MW, according to a worldwide wind energy research [4]. Based upon research and development (R&D) in the area of wind energy technology, much advancement has been made i.e., micro-meteorology, aerodynamics, and structural design improvement, to enhance the energy production of turbines in the last few decades. The improvements include increasing their output power and reducing their weight and noise. Wind energy has advantages over other energy technologies based upon its maturity, infrastructure, and economic cost. The wind turbine is a device that mainly

Nomenclature

CAD	Computer aided design	N	Number of blades
CFD	Computational fluid dynamics	ρ	Fluid density (kg/m^3)
HAWT	Horizontal axis wind turbine	θ	Azimuth angle (deg)
MRF	Multiple reference frame	V	Wind speed (m/s)
PISO	Pressure implicit with splitting of operators	λ	TSR
RANS	Reynolds averaged Navier-Stokes	C_p	Power coefficient
R&D	Research and development	ω	Angular velocity (rad/s)
TSR	Tip speed ratio	A	Swept area (m^2)
VAWT	Vertical axis wind turbine	c	Chord length (m)
CCS	Carbon capture & storage	P	Output power (Watt)
Solar PV	Solar photovoltaic	W	Relative flow velocity
CSP	Concentrated solar power	R	Rotor radius
V_n	Normal velocity (m/s)	α	Angle of attack (deg)
V_c	Chordal velocity (m/s)	σ	Solidity
V_a	Axial velocity (m/s)	μ_t	Turbulent viscosity (kg/ms^{-1})
τ	Stress tensor	F_{ta}	Tangential force (N)

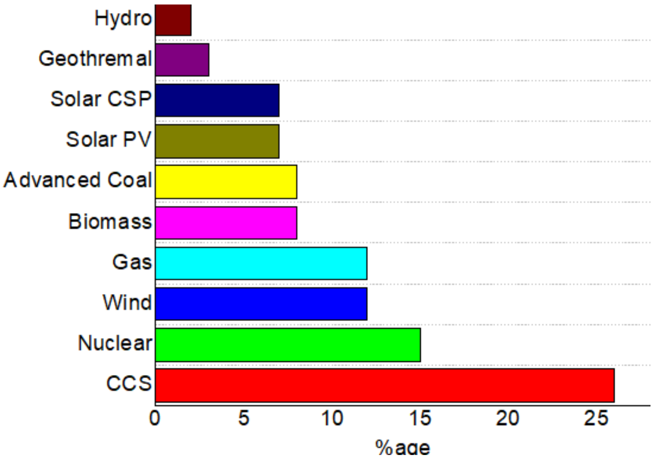

Figure 1. CO_2emission reduction by different energy sectors [2].

consists of a rotor hub and blades. Incoming airflow is deflected by the rotor that results in the creation of force on rotor blades followed by the generation of shaft torque. The attached rotor rotates about its axis and electricity is generated with the help of a generator and mechanism installed within it. The output power can be enhanced by selecting appropriate wind sites, suitable power analysis machines, and efficient energy storage devices [1,2,5]. The power coefficient (C_p), which may be calculated from the ratio of the power generated by the wind turbine to the power that is currently available in the wind, is the fundamental characteristic connected to wind energy. Calculation of the power density factor will permit wind turbines to be positioned at effective sites for producing electrical power. The relationship between the C_p and output power is given by **Equation 1**.

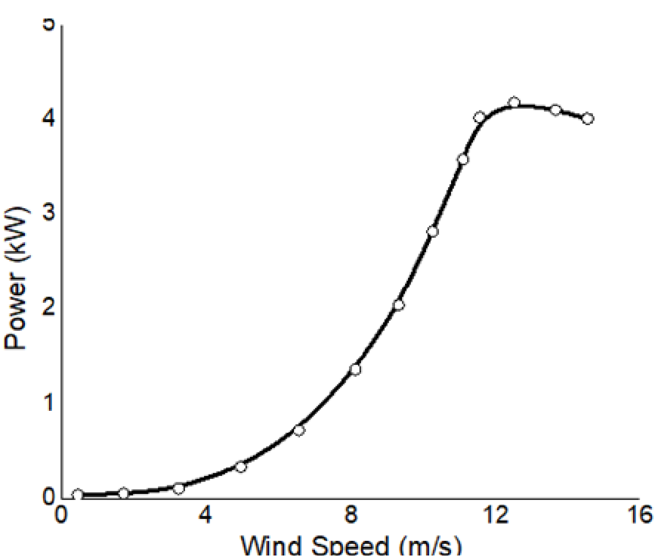

Figure 2. The variation of output power with wind speed for a wind turbine of 4 kW [7].

$$P = \frac{1}{2}\rho A V^3 C_P \quad \text{.............................} \quad (1)$$

where C_p is the power coefficient, ρ is the density of the air, V is the wind speed, and A is the swept area of the turbine [6]. In contrast to other machines, wind turbines can only produce energy in response to the wind that is immediately accessible, therefore they cannot convert all of the wind's energy into work. The Betz limit, which states that a turbine cannot collect more than 59.3% of the power inside a continuous stream of air of equal area, establishes the maximum energy that may be obtained from a certain wind flow. The maximum value of the C_p is reduced by aerodynamic drag, pressure variations in the turbine plane, wake rotation downstream of the rotor, number of blades, and tip loss values. Output power depends on the wind speed, density and blade swept area. A typical variation of output power with speed for a 4-kW wind turbine is shown in **Figure 2**. The C_p, which measures the aerodynamic efficiency of wind turbines, can be determined using the TSR calculated by **Equation 2**. This ratio serves as a valuable indicator of the relationship between the rotational speed of the turbine's blades and the velocity of the wind passing through them.

$$\lambda = \frac{\omega R}{V} \quad \text{..................................} \quad (2)$$

where ω is rotational velocity, R is turbine radius, and V is wind speed. Another often used term for measuring the area occupied by a VAWT is solidity. Solidity may be determined from the ratio of the product of chord length with the number of blades to radius of the rotor as provided by **Equation 3** [8].

$$\sigma = \frac{N_C}{R} \quad \text{..................................} \quad (3)$$

where σ is solidity, R is turbine radius, c is the chord length of the turbine blade, and N is the number of blades. The maximum performance of the turbine can be deter- mined by the variation of solidity. At lower TSR values, there is a very weak interaction between blades and airflow passing through the swept area; however, blades interact strongly with the wakes at high TSR.

This study seeks to support current initiatives to enhance the aerodynamic performance of vertical axis wind turbines (VAWTs). Despite the significant advancements in wind turbine technology, there is still a need for further enhancement in VAWTs to maximize their efficiency and power generation capabilities. Therefore, this study focuses on investigating the aerodynamic characteristics of three different VAWT designs: the airfoil, H-Rotor Darrieus, and Savonius wind turbines. To gain insights into the aerodynamic behavior and performance of these VAWT configurations, computational fluid dynamics (CFD) analysis was employed. CFD simulations enable a detailed examination of the flow patterns, pressure distributions, and forces acting on the turbine blades and surrounding air. By accurately modeling the complex fluid dynamics involved, CFD analysis provides valuable information on the performance of VAWTs under various operating conditions. The findings of this research will contribute to the existing body of knowledge on VAWT aerodynamics and provide practical insights for wind turbine designers and engineers. Ultimately, the aim is to facilitate the development of more efficient and economically viable VAWT systems, thus contributing to the advancement of renewable energy technologies and their wider adoption in the pursuit of sustainable energy solutions.

The following is a breakdown of the paper. **Section 2** presents the classifications of wind turbines including various horizontal axis wind turbines (HAWTs), vertical axis wind turbines (VAWTs), and aerodynamic parameters. **Section 3** presents the computational analysis and results obtained during the research. Finally, **Section 4** presents the conclusions.

2. CLASSIFICATION OF WIND TURBINES

The kinetic energy of the wind is transformed into electrical energy via wind turbines. Depending on their design and geometric configurations, both HAWT and VAWT are commercially available in a range of sizes and capacities. Small turbines can be used as a backup power source or to operate traffic lights, but bigger turbines are often employed for industrial and home applications. Over the past few decades, the sizes of wind turbines have increased significantly, reaching a scale of 100, while associated energy costs have decreased to less than 10 [2,9,10]. The HAWTs are the most typical and have been in use for decades. In VAWT, the turbine rotates around a vertical axis, which means that its blades spin in a plane perpendicular to the ground surface. The rotation axis of the VAWT remains vertical (upright) and does not change its orientation with respect to the ground. As the wind blows, the turbine's blades capture the wind's energy, causing the turbine to rotate around its vertical axis. In the near future, wind energy technology will be leading as a result of recent R&D effort in the design and development of VAWTs [11]. A sketch diagram of HAWT and VAWT concerning their axis of rotation and incoming flow is shown in **Figure 3**. The basic difference between these two types as shown in the figure is that VAWT can take incoming flow from any direction around its axis which is called omni-directional [12].

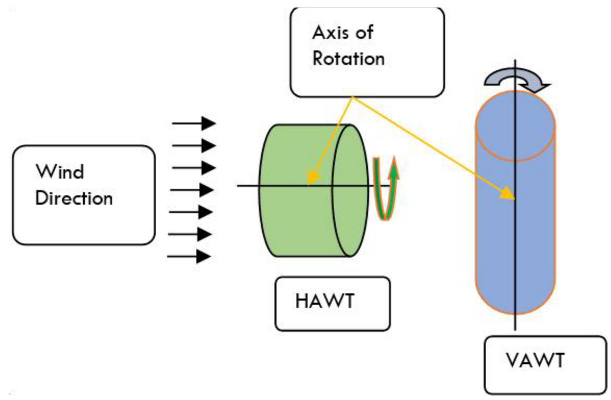

Figure 3. Sketch diagram showing direction of rotation of HAWT and VAWT with respect to incoming airflow [4]

2.1. HORIZONTAL AXIS WIND TURBINE

HAWTs are often employed for a variety of power projects across the world. The axis of rotation of wind turbines in these categories is always horizontal or parallel to the ground. These turbines continue to be popular because they have higher theoretical efficiency [13,14]. **Figure 4** depicts a schematic of the HAWT's main parts. Wind sensors and a yaw mechanism work together to regulate the position of the rotors, which are mounted at the top of the tower and directed into the wind [15]. The majority of turbines contain a gearbox that is utilized to increase the blades' sluggish rotation, making it more practical to drive electrical generators [16]. Due to the influence of the wake on the turbine located downstream, it is not feasible to construct them in close proximity. As the flow passes through the turbine, it experiences a reduction in velocity, accompanied by a significant rise in turbulence levels. From the hub center side, it is discovered that the wake effects are quite powerful near to the swept region and weaken towards the blade tip [17]. HAWTs are extremely sensitive to the effects of turbulence and the direction of the wind. However, they are extremely effective in generating wind energy from the available wind. HAWTs have certain disadvantages, including considerable tower wobble, requirement of large space for blade operation, high dependence on wind direction,

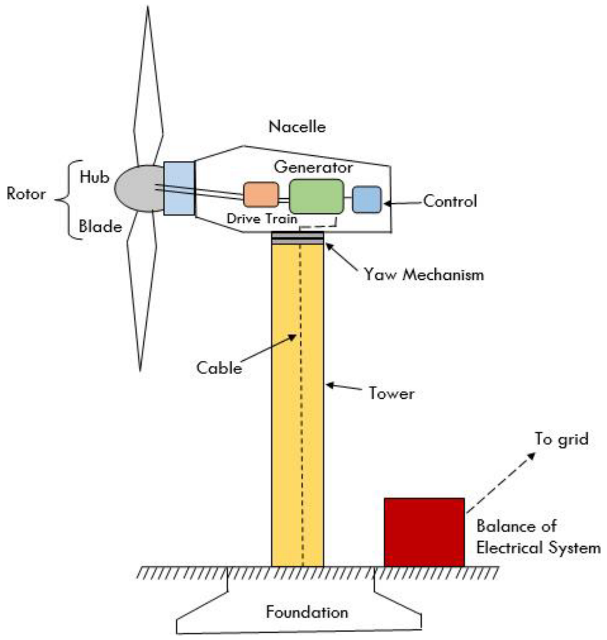

Figure 4. Major components of HAWT; the major component nacelle is positioned behind the rotor to align with the incoming airflow. The rotor of the HAWT rotates with the assistance of a yaw mechanism [4]

Table 1. Salient features of different configurations of HAWTs [18, 19]

S No.	Turbine type	Salient features
1	Tulipo	It can easily rotate at low-speed ranges. It produces less noise, vibrations and involves less maintenance due to fixed stall blades.
2	Swift	Small wind turbine with thin blades. It produces less vibration and has noise diffusion capability.
3	Fortis Montana	A very less noise-producing turbine with very low tip speed. Due to its small size, it can be used for domestic power requirements.
4	Eclectic	Designed for low-speed operations and results in efficient power production.
5	Scirocco	Installed with variable pitch blades.

birds and airplane obstructions, and maintenance concerns resulting from design combinations [18,19]. HAWTs' unique design enables them to fully rotate under constant flow situations and capture the maximum amount of wind energy [20]. **Table 1** lists the key characteristics of the various HAWT design setups.

2.2. VERTICAL AXIS WIND TURBINE

The axis of rotation in these kinds of wind turbines continues to be upward or vertical to the ground. According to recent studies on the design and development of VAWTs, these devices may dominate wind energy technology in the coming decades. These turbines do not require wind from a particular direction to operate rather wind can be accepted from any direction resulting in electrical power generation without being affected by yaw moment [21,22]. These are the most effective and efficient selection of power generation in high wind and turbulent flow areas. Another advantage of these turbines that due to less height they do not get much affected by birds or aircraft activities. Moreover, power storage and controlling accessories can be placed on the ground [4,15,23]. VAWTs are being used in different design configurations worldwide because of their low manufacturing cost, easy installation, and less maintenance. For most populated areas these are considered a very efficient solution because these can be installed in small available space and their suitability for small scale utilization [24]. However, VAWTs are not very effective due to some of their drawbacks i.e., starting torque, low lift and drag forces, and poor efficiency rating, etc. [25]. The research in this field is still going on to overcome similar problems and to enhance the performance parameters. There are many types of VAWTs being used in different countries i.e., Giromill turbines, Darrieus turbines, Cross-flow wind turbines, Savonius turbines, Zephyr, and Gorlov helical turbines etc.

2.2.1. VARIOUS COMPONENTS OF VAWT

In the process of designing and fabricating a VAWT, the key components typically required include the foundation, tower, rotor, hub, blades, shaft, generator, and connecting rod (**Figure 5**). These components collectively contribute to the efficient operation and construction of the VAWT [4,26,27]. Below is a brief summary of the components:

(i) Rotor blades: These are used to capture the wind energy and to transform it into kinetic energy through the hub's circulation. The rotor design depends on the type of blades because it has a great effect on wind energy capturing.

(ii) Rotor: It is used to transform the available wind energy into mechanical power.

(iii) Foundation: Prevent the turbine from any damage during high wind speed.

(iv) Tower: It is used to support the rotor and hub assembly.

(v) Hub: The attachment point for the blades is at the rotor's center. Most often, it is composed of steel and cast iron. Some VAWT designs require two hubs on the bottom and upper sides because the blades are connected at two different places.

(vi) Generator: The mechanical energy produced by the rotor is converted into electrical power by using a generator.

(vii) Shaft: Turbine blades are attached to a shaft that revolves with the blade.

2.2.2. AERODYNAMICS OF H-ROTOR DARRIEUS VAWT

The aerodynamics of H-Rotor Darrieus VAWTs present a fascinating and intricate field of study, despite their apparent simplicity. Understanding the complex flow patterns and forces acting on the H-Rotor Darrieus design re- quires a comprehensive analysis. **Figure 6** provides a visual representation of the flow velocities associated with both the upwind and downwind sides of the turbine. This diagram sheds light on the intricate interactions between the wind and the turbine blades, helping researchers and engineers unravel the aerodynamic phenomena involved. By delving deeper into the aerodynamics of H-Rotor Darrieus VAWTs, their performance, efficiency, and overall design can be enhanced, leading to advancements in harnessing wind energy effectively and sustainably [28].

The velocity component in the normal (V_n) and chordal (V_c) directions may be calculated from the velocity triangle as provided in **Equations 4** and **5** when taking into account the axial flow occurring on the turbine blade.

$$V_c = R\omega + V_a \cos\theta \quad \ldots\ldots\ldots\ldots\ldots\ldots\ldots\ldots\ldots (4)$$

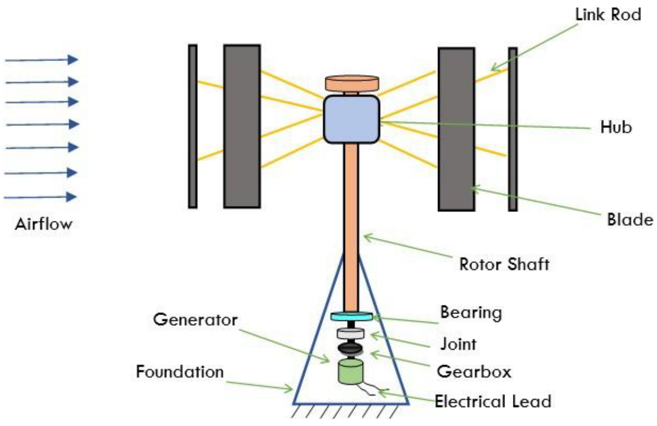

Figure 5. Major components of VAWT; since most of the components are positioned on the ground, therefore, installation and maintenance tasks are made easier [4]

$$V_n = V_a \sin\theta \quad \ldots\ldots\ldots\ldots\ldots\ldots\ldots\ldots\ldots\ldots (5)$$

where θ stands for azimuth angle, ω for rotational velocity, V_a for axial velocity through the rotor, and R for the radius of the turbine. The figure may be used to calculate the relative flow velocity (W), as demonstrated by **Equation 6**.

$$W = \sqrt{V_n^2 + V_c^2} = \sqrt{(V_a \sin\theta)^2 + (R\omega + V_a)^2} \quad \ldots (6)$$

Equation 7 represents the variation of the local angle of attack (α) for an airfoil blade. It is calculated as the arctangent of the ratio between the normal velocity component (V_n) and the chordal velocity component (V_c). This equation allows for the analysis of the blade's aerodynamic performance and how the angle of attack changes with different flow conditions during rotation.

$$\alpha = \tan^{-1}\frac{V_n}{V_c} = \tan^{-1}\frac{V_a \sin\theta}{R_\omega + V_a \cos\theta} \quad \ldots\ldots\ldots (7)$$

The tangential force coefficient (C_t) is determined by combining the tangential components of lift and drag forces (**Equation 8**). On the other hand, the normal force coefficient (C_n) is obtained by summing up the lift and drag normal components (**Equation 9**). These coefficients represent the resulting forces acting on the object and are vital in analyzing its aerodynamic characteristics.

$$C_t = C_l \sin\alpha - C_d \cos\alpha \quad \ldots\ldots\ldots\ldots\ldots\ldots\ldots\ldots\ldots (8)$$

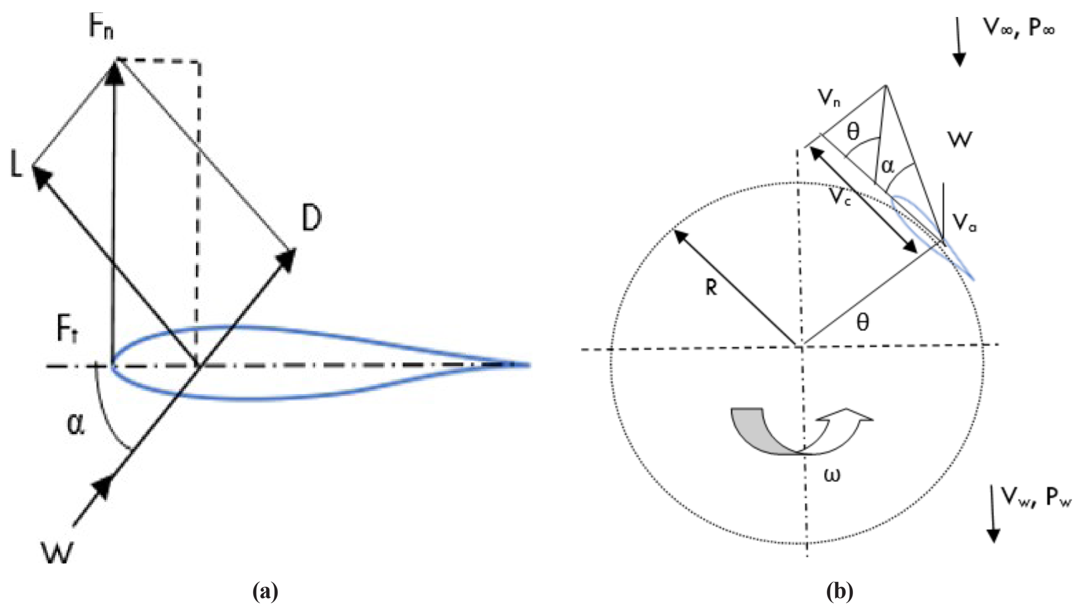

Figure 6. (a) The forces and associated flow velocities acting on the blade airfoil, (b) Blade position in turbine rotor [4]

$$C_n = C_l \cos\alpha + C_d \sin\alpha \quad (9)$$

The tangential and normal forces acting on a wind turbine blade vary depending on the azimuth or orbital position. To determine the average value of the tangential force (F_{ta}), **Equation 10** can be utilized. This equation allows for the calculation of the average tangential force by considering the forces at different orbital positions.

$$F_{ta} = \frac{1}{2\pi}\int_0^{2\pi} F_t(\theta)d\theta \quad (10)$$

The total torque (Q) and output power (P) for the N number of blades may be calculated using **Equations 11** and **12**, respectively.

$$Q = N \cdot F_{ta} \cdot R \quad (11)$$

$$P = Q \cdot \omega \quad (12)$$

3. FLOW FIELD ANALYSIS OF VAWTS

There are many design configurations of VAWTs that have been developed and being utilized by different countries on commercial as well as domestic levels [9]. In this paper, the flow field analysis of the Savonius rotor and H- Rotor Darrieus VAWT utilizing CFD has been carried out. Variation of output power with respect to free stream velocity and geometric parameters for both the design configurations have been estimated. Based on the obtained results, the comparison has also been carried out to recommend a favorable design. The details of the analysis will be discussed in subsequent sections.

3.1. H-ROTOR DARRIEUS TURBINE

H-Rotor Darrieus is a lift-based turbine having straight blades configuration also called Giromill turbine. This turbine is being used in two or more blades configuration installed with different blade sizes and aerodynamic structures [29,30]. A pictorial view of H-Rotor Darrieus turbine is shown in **Figure 7**. The blades are designed to provide a fixed or variable pitch to make them more effective in highly turbulent flows. These types of variable pitch blade configurations are used to reduce the starting torque issues and can be used at domestic levels. Another advantage of these turbines is that they produce very little noise and have a good C_p at high TSR values [31]. In the current study, a fixed-pitch design has been selected to analyze the flow parameters around the blade profile and nearby influencing domain. Fixed blades installed on these turbines are having comparatively simple designs but have issues of poor starting torque. Many investigators have deliberated to optimize the design of these turbines based upon parameters i.e., aerodynamic

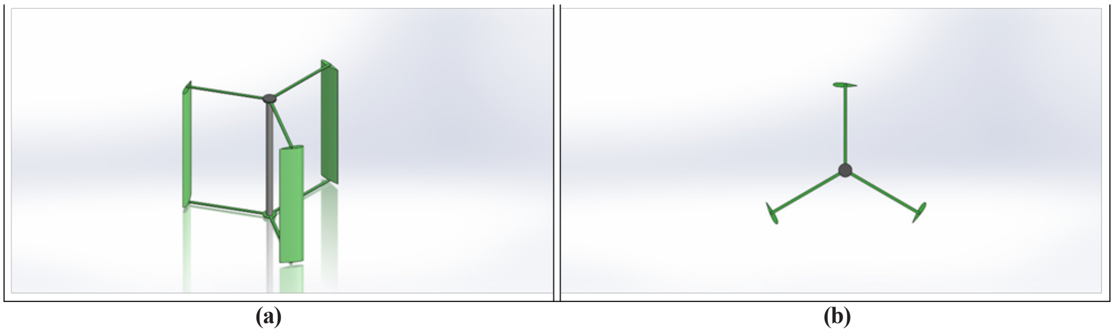

Figure 7. CAD model of three-dimensional H-Rotor Darrieus turbine (a) isometric view (b) top view.

effects, airfoil shape, guide vane addition to enhance C_p, and self-starting torque improvements, etc. [32].

Over the past few decades, numerous experts have conducted extensive study to improve output power and optimize design configurations. Hussen *et al.* [33] conducted research on the creation of VAWTs to produce electrical output power while operating in adverse weather circum- stances. Three-dimensional static studies were conducted on straight and twisted blade configurations comprising three blades, utilizing the NACA0018 airfoil. Using numerical analytic techniques, these studies were conducted at various wind speeds ranging from 3 to 15 m/s. The study focused on analyzing the blades' performance and properties, experimenting with various materials like aluminum, glass fiber, and carbon fiber. This enabled an assessment of how these different blade materials affected the overall performance of the wind turbine system. With the extra benefit of a low-speed starting, analysis of various configurations reveals that utilizing twisted blades can enhance average output power by up to 8.75%. CFD is regarded as a useful and potent method for researching complicated and unstable flow issues linked to wind turbines [34]. The performance of straight and helical blade VAWTs was compared by Alaimo *et al.* [35] using CFD. They solved the Reynolds averaged Navier-Stokes (RANS) equations for this purpose. In their study, they utilized a NACA0021 blade airfoil with a chord length of 0.3 m and a turbine radius of 0.99 m. At different TSR, a two-dimensional dynamic analysis was performed, and torque, drag, as well as lift coefficients were the outcomes. The analysis focused on studying the flow characteristics over the rotor blade concerning its azimuth position across a range of revolutions. The findings of a 3D static and dynamic study confirmed that utilizing helical blades increased torque coefficient values. Sabaeifard *et al.* [36] conducted experimental testing and CFD simulations on the H-Rotor Darrieus turbine. The study aimed to assess the effect of various design factors, including airfoil type, number of blades, solidity, and TSR. Transient simulations were performed using the multiple reference frame (MRF) and k-ω turbulence model. The researchers examined the C_p at different TSR values, utilizing NACA0018 and DU 06-W-200 airfoils. The influence of solidity and the num- ber of blades on C_p was also investigated. The analysis re- vealed the maximum C_p achieved by the optimized turbine parameters (DU 06-W-200 airfoil, solidity: 0.3, number of blades: 3) as > 0.30 at a TSR of 3.5, respectively.

3.1.1. AIRFOIL SELECTION

The wind turbine blade's cross-sectional area functions as an airfoil, producing aerodynamic forces as a result of fluid motion around it. The maximal rotor power and expected aerodynamic performance determine the blade's length and width. For various wind turbines, several airfoils, such as the NACA, DU, BE, and NREL series, have been employed. In the present study, the flow field surrounding the Darrieus blade has been 2D analyzed using the sliding mesh approach. Based upon the performance analysis carried out by Sabaeifard *et al.* [36], DU 06-W- 200 airfoil was selected for the H-Rotor Darrieus turbine. The profile of the selected airfoil is shown in **Figure 8**. Some of the aerodynamic

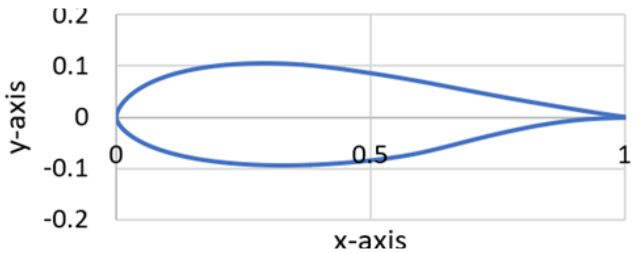

Figure 8. The profile of DU 06-W-200 airfoil

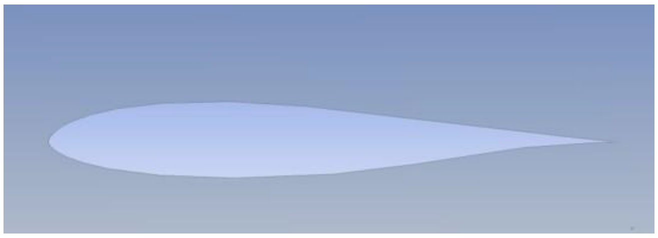

Figure 9. Airfoil geometry developed in ANSYS design modeler

Table 2. Aerodynamic characteristics of DU 06-W-200 airfoil [37]

S No.	Parameter	Value
1	Maximum thickness	0.198 at 31.1% chord
2	Maximum camber	0.005 at 84.6% chord
3	Reynolds number	50,000
4	Cl_{max}	0.625 at $\alpha = 3.5^{\circ}$
5	$(C_l/C_d)_{max}$	11.05 at $\alpha = 3.5^{\circ}$
6	Zero-lift angle of attack	-3.75°
7	Applications	Small scale VAWTs

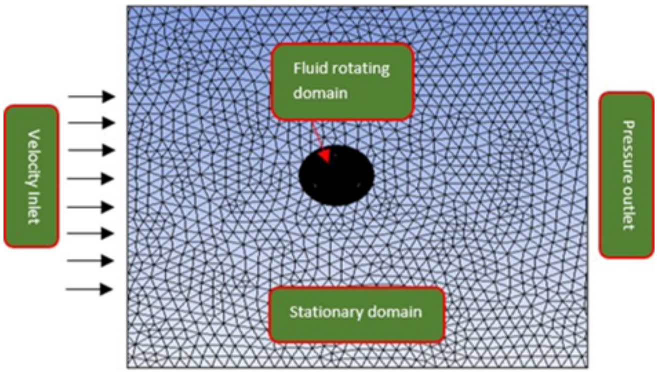

Figure 10. Circular and rectangular domain around the blades

characteristics of selected airfoil are given in **Table 2**.

3.1.2. COMPUTER AIDED DESIGN AND CFD ANALYSIS

To carry out computational fluid dynamic analysis, airfoil coordinates were imported from airfoil tools and geometry was developed in an ANSYS design modeler. The problem under consideration involves modeling of moving element (rotor blade and the fluid area) and the stationary portion (rest of the domain). MRF is a quite strong and effective steady-state, CFD modeling procedure to simulate moving parts. MRF is one of the methods for problems relating to multiple zones. It is a steady-state estimation in which discrete cell zone moves at dissimilar rotating or translation speeds. It assumes that a designated volume rotates continuously and the non-wall boundaries serve as the rotational surfaces. For flow conditions where there is no interface among stationary and moving parts, it is recommended to use a rotating reference frame. MRF is comparable to running a rotating simulation and then examining the outcomes at the moment corresponding to the place of the rotor within it [38]. An alternative to MRF is the sliding/moving mesh procedure, which simulates the flow with strong interactions among the moving volume and the nearby static volumes. However, in some cases, the moving mesh procedure has robustness problems due to its dependence on connection and calculations between the rotating and stationary volumes [39]. The sliding mesh approach was used in the current study to examine the flow along the blade surface. The blade surface of the cambered airfoil developed using ANSYS software is shown in **Figure 9**.

Three blades geometry along with circular domain around each of the blade airfoil was developed as shown in **Figure 10**. The large circular outer domain was generated to simulate the flow in the domain and the rectangular domain to establish boundary conditions. The flow in the respective moving cell zone was solved by applying the Navier-Stokes equations, which consider the centripetal and coriolis acceleration in the momentum equation. Navier-Stokes equations are fundamental partial differential equations in fluid dynamics, describing the motion of fluids by accounting for the conservation of momentum and the relationship between fluid velocity, pressure, and viscosity. They play a critical role in understanding and modeling fluid behavior in various scientific and engineering applications [40,41]. At the interfaces between the cell zones, the transformation of the local reference frame was carried out to allow flow parameters in a single zone to be used to compute fluxes at the edge of the adjacent zones [42].

The computational simulation in **Figure 11** employs specific boundary conditions to accurately represent the flow behavior around the wind turbine. The velocity inlet condition defines incoming flow velocity at the computational domain's inlet. Meanwhile, the pressure outlet condition manages flow pressure at the domain's exit. Utilizing a symmetry condition takes advantage of symmetry and reduces computational effort. The airfoil sur- face is treated as a stationary wall to accurately capture flow-airfoil interaction. An interface condition is implemented to connect rotating and stationary domains seamlessly. The rotating domain specifies rotational behavior, while the stationary domain represents the non-rotating section. These carefully chosen boundary conditions ensure reliable results, accurately simulating flow behavior, and facilitating comprehensive aerodynamic analysis under various operating conditions. After the generation of circular and rectangular domains around the three-blade surfaces, the triangular mesh was generated using the automatic mesh technique and patch-independent

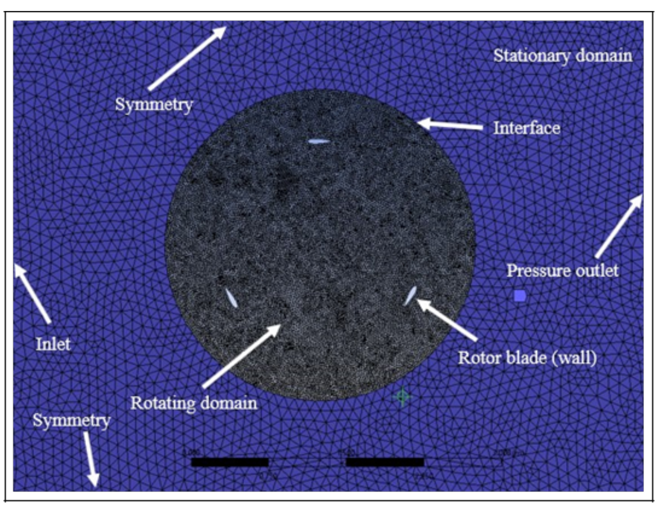

Figure 11. Mesh generated around the airfoil and fluid domain

method. **Figure 11** shows the refine mesh around the airfoil (element size of 0.005 m) and coarse mesh in the rectangular domain. The reason for the refined mesh was to capture the more accurate flow parameters close to the boundary layer. Fluent is an efficient two/three-dimensional mesh solver, which assumes multigrid solution algorithms. The pressure and density-based solver are available in the Fluent module. The pressure-based solver was created for low-velocity incompressible flows, whereas the later solution simulates high-speed compressible flows [39]. Inertial frame of reference is frequently used to solve the fluid flow equations. Due to incompressible flows at this instance, a pressure-based strategy was used. An algorithm that belongs to the general class of strategies known as the prediction technique is paid by the pressure-based solver. By solving a pressure equation, the projection approach satisfies the velocity field constraint of conservation of mass.

In order to ensure that the velocity field's modification by the pressure upholds the continuity principle, the pressure equation is derived from the momentum and continuity equations. ANSYS Fluent provides many selections of turbulence models. The selection of turbulence model is dependent on considerations such as conventional repetition for a detailed class of problem, physics encompassed in the flow, existing computational resources, the accuracy level, and the availability of total time for the simulation [43]. The turbulence model employed in this study was the standard k-ϵ model with standard wall condition. This model uses two separate transport equations to independently determine the turbulent kinetic energy (k) and its dissipation rate (ϵ). This approach has been widely utilized by various researchers [44–46] and has demonstrated improved accuracy. The results obtained from this model showed good agreement between experimental data and the CFD predictions for the target function, C_p. Considering the successful application of this model in wind turbine analysis and after reviewing relevant literature, it was chosen for the current study as well.

3.1.3. PARAMETERS SETTING AND BOUNDARY CONDITIONS

To analyze the flow around the turbine blades using MRF and sliding mesh technique, boundary and cell zone conditions at the inlet, outlet, circular domain, and rectangular domains were selected as per the details given in **Table 3**.

Table 3. Parameters setting and boundary conditions [10,47]

S No.	Parameter	Value
1	Algorithm	PISO
2	Flow model	k-ε
3	Viscosity ratio	10
4	Fluid density	1.225 kg-m^{-3}
5	Turbulent intensity ratio	0.05
6	Inlet	Velocity: 0–12 m/s
7	Outlet	Pressure outlet
8	Rotor rpm	60–150

After setting boundary and cell zone conditions, the solution was initiated, and to capture steady-state simulations the solution was run for about 2000 iterations.

To perform transient flow analysis, an alternate approach (sliding mesh) was adopted and keeping the same cell zone boundary conditions in mesh motion settings. The residuals are run by defining the appropriate number of time steps and time step size. At each time step, Fluent iterates until the solution are converged for the existing time step (or the max number of repetitions per step time is reached), then moves on to the next time step and iterates until the solution is converged. Simulations were run and velocity contours at different time intervals were recorded in the sliding mesh technique. The velocity con- tours and vector results were obtained as shown in **Figures 12a** and **12b**, respectively. Contours show the variation of velocity magnitude with the rotation of turbine blades. Areas of wake region and variation of velocity values can easily be identified from the simulations.

3.1.4. ANALYSIS OF THREE-DIMENSIONAL H-ROTOR DARRIEUS TURBINE

H-Rotor Darrieus turbine is a lift-based wind turbine installed with constant cross-sectional area blades. It has a very low self-starting capability. However, its efficiency improves at high TSR ranges, and it produces minimal noise. Therefore, it can be installed in rooftop locations. Different design configurations of these turbines have been developed with two, three, and four blades. Some of the configurations are also modified with variable pitch design [48]. Theoretical modeling of this category indicates that the maximum C_p would expect to be more than 0.4 and these can produce power up to 10 kW. To analyze the flow field around three-dimensional H-Rotor Darrieus turbines, geometry having a straight blade with NACA0021 airfoil with a chord length of 95 mm was developed using computer-aided design (CAD) software and the same was imported in ANSYS Fluent. The geometric parameters were selected based upon experimental testing performed by a researcher [49]. The geometry consists of three blades with joints at the upper and lower ends (**Figure 7**). Once the 3D model for the computational domain around the geom meshing sizes of turbine blades and domain were specified. To get precise simulation results, element sizes must be quantified well. The computational domain, boundary conditions of H-Rotor Darrieus are shown in **Figure 13** [6].

3.1.5. GRID INDEPENDENCE TEST

Grid independence testing is a crucial step in CFD

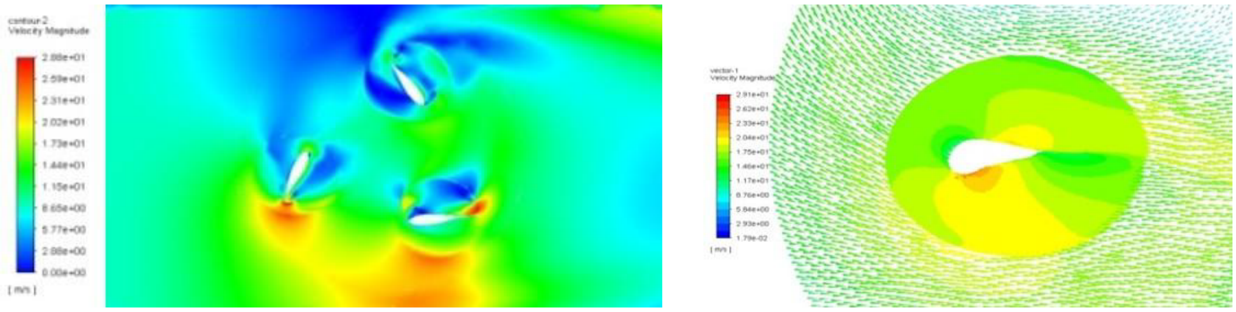

(a) (b)

Figure 12: (a) Velocity contours around the blade and outer domain, (b) Velocity vectors around blade airfoil

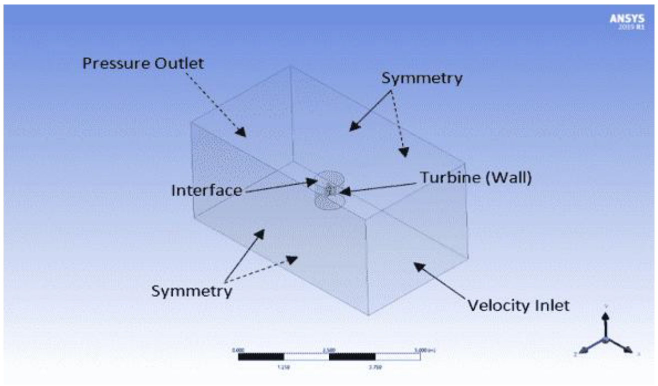

Figure 13: Computational domain and boundary conditions of H-Rotor Darrieus.

analysis, where different grid resolutions are employed to assess the sensitivity of numerical results. By systematically varying the grid size while keeping other parameters constant, it can be determined if further grid refinement significantly affects the outcomes. The goal is to achieve grid convergence, where the solution approaches a consistent value as the grid is refined. This test helps strike a balance between computational cost and accuracy, ensuring the reliability of CFD simulations and enabling informed engineering decisions [12]. To select the output parameter in this test, in the parametric window of the mesh module, the number of divisions of all the turbine faces were selected followed by the selection of nodes and elements option in mesh statistics. Mesh size was changed from coarse to various levels of refinement. The number of nods and elements obtained for each refinement level is shown in **Table 4**.

Table 4. Mesh refinement level and number of nodes/elements

Refinement level	Nodes (Mil)	Elements (Mil)
Coarse mesh	0.09	0.51
1	0.18	1.53
2	0.62	2.31
3	1.31	3.83
4	2.72	5.14

A mesh was created with a transition pattern of 1:1 and a growth rate of 1.4. The initial cell size close to the wall was determined according to the y+ value, ensuring it remains below 5 for the viscous sublayer [50–52]. This y1 value was computed based on the design wind speed and maximum rotational velocity. The element size adjacent to the walls was set to 0.005 m. The computational domain had over 2 million total mesh elements, providing a grid- independent solution and keeping the maximum skewness below 0.6. In the beginning, the computational domain as a whole was built using a coarse mesh. Subsequently, the mesh was refined by defining different levels of refinement. To analyze the grid effects, the C_p generated by the turbine rotor was selected as an effective parameter for different refinement levels. The same set of requirements were used to solve each refinement level in Fluent. The results obtained for various levels of refinement are shown in **Figure 14**. The figure highlights the independence of mesh size beyond this design point because there was no appreciable quantitative difference in the outcome after refinement level 2 and the same was selected for the further simulations.The mesh created

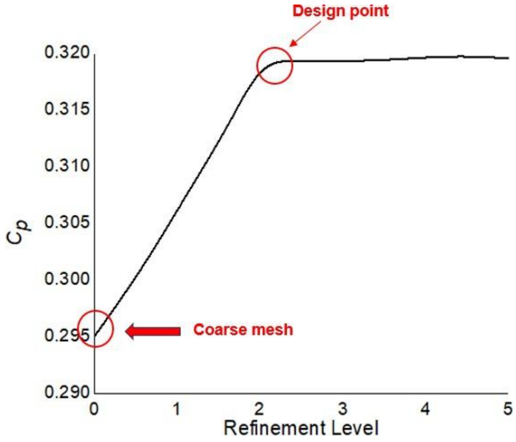

Figure 14: The figure depicts the variation of the Cp as a function of the grid refinement levels. After refinement level 2, the parameter is constant, indicating that the grid size is independent.

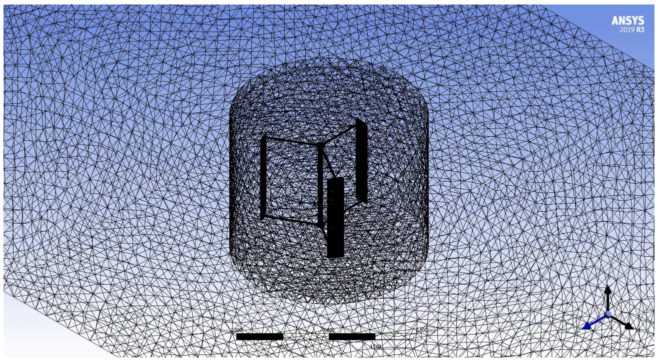

Figure 15. Refined mesh generated around turbine blades.

around the turbine blades, the inner rotating domain, and the outer stationary domain are shown in **Figure 15**. The computational domain was exported to the Fluent module after the mesh had been successfully created.

3.1.6. CFD FORMULATION

The sliding mesh approach was used to perform the transient analysis. This method created many zones around the geometry, and by making use of the interfaces, mesh motion is made easier. A set of differential equations de- scribe how fluid flow, energy, and momentum are physically transported. At certain boundary conditions, a set of algebraic equations were used to solve the Navier-Stokes, turbulent, and continuity equations in their finite-difference versions [53]. The flow was regarded as being incompressible and having constant viscosity using built-in Fluent programs while solving the differential equations. The equations in the form of conservation of mass and momentum in vector form (Navier-Stokes equation) are represented by Equations 13 and 14, respectively [44].

$$\nabla \cdot \rho \vec{v} = 0 \quad \text{(13)}$$

$$\frac{\partial}{\partial t}(\rho \vec{v}) + \nabla \cdot (\rho \vec{v}\vec{v}) = -\nabla P_s + \rho \vec{g} + \nabla \cdot \overline{\overline{\tau}} \quad \text{(14)}$$

In the context of this discussion, with P_s representing static pressure, ρ denoting fluid density, $\vec{v}$ representing fluid velocity as a vector, τ as the stress tensor, and $\overrightarrow{\rho g}$ representing gravitational force, the application of Stokes' theory of Newtonian fluids allows us to express the stress tensor using **Equation 15**.

$$\overline{\overline{\tau}} = \mu(\nabla \vec{v} + \nabla \vec{v}^T - \frac{2}{3}\nabla \vec{v} I) \quad \text{(15)}$$

Using a two-equation turbulence model, the rate of dissipation and kinetic energy were calculated. Various turbulence models are available in ANSYS Fluent package i.e., $k\epsilon$, $k\omega$, and SST, etc. Among the available packages, $k\epsilon$ along with realizable is considered to be the most efficient as it provides more accurate results and very few convergence issues are faced in this model. Moreover, this model is also accurate and fast to predict separate flow from the wind turbine. When a turbulence model is said to be "realizable," it means that it adheres to certain mathematical constraints on the Reynolds stresses that are compatible with the flow physics. The transport equations of the selected model for the rate of dissipation and kinetic energy are given in Equations 16 and 17 [44,45,54].

$$\mu_t = \frac{\partial}{\partial t}(\rho k) + \frac{\partial}{\partial x_i}(\rho k u_i) = \frac{\partial}{\partial x_i}\left[\left(\mu + \frac{\mu_t}{\sigma_k}\right)\frac{\partial k}{\partial x_j}\right] + P_k + P_b - \rho\varepsilon - YM + Sk \quad \text{...(16)}$$

$$\frac{\partial}{\partial t}(\rho\epsilon) + \frac{\partial}{\partial x_j}(\rho\epsilon u_j) = \frac{\partial}{\partial x_j}\left[\left(\mu + \frac{\mu_t}{\sigma_\epsilon}\right)\frac{\partial \epsilon}{\partial x_j}\right] + \rho C_l S\epsilon - \rho C_2 \frac{\epsilon^2}{k + \sqrt{v\epsilon}} + C_{l\epsilon}\frac{\epsilon}{k}C_{3\epsilon}P_b + S_\epsilon \quad \text{(17)}$$

where turbulent viscosity (μ_t), constant (C_1) can be determined by **Equations 18** and **19**.

$$\mu_t = \frac{\rho C_\mu k^2}{\varepsilon} \quad \text{(18)}$$

$$C_1 = \max 0.43, \frac{\eta}{\eta + 5} \quad \text{(19)}$$

where,

$$\eta = S\frac{k}{\varepsilon} \quad \text{(20)}$$

Where G_k denotes the amount of kinetic energy generated during the process as a result of the average velocity gradient. The constant σ_ϵ and σ_k are representing the turbulent Prandtl numbers of dissipation rate and kinetic energy. The values of these constants are taken as 1.2 and 1.0, respectively. During the analysis, it was also assumed that thermophysical properties remain constant hence, the energy equation was not executed. The compression work was also assumed as negligible in a three-dimensional flow field. To find the maximum value of C_p, TSR values for various rotational velocities were calculated. Numerical simulations were carried out utilizing the sliding mesh technique combined with the unstructured-grid finite volume approach after choosing the k–ϵ flow model and adding boundary constraints. The inner rotational domain's uneven flow may be transferred to the outer stationary domain through the sliding interface with the aid of the sliding mesh approach [47]. For transient or unstable calculations, the pressure implicit

Table 5. Time step, moment, and power coefficient (C_p)

S No.	Time step (s)	Moment (n-m)	C_p
1	1	12.24	0.357
2	0.5	18.53	0.333
3	0.1	23.21	0.327
4	0.05	23.27	0.320
5	0.01	24.24	0.319
6	0.005	24.25	0.320
7	0.001	24.06	0.321

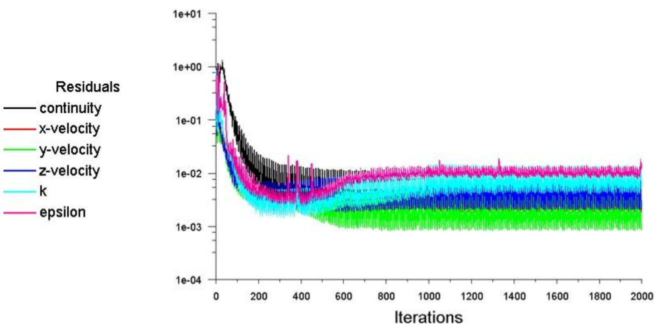

Figure 16. Convergence check; the figure shows that after 1000 iterations, solution was converged.

with splitting of operators (PISO) method was used during the analysis. Convective components of the turbulence and momentum equations were subjected to a second-order discretization technique in order to achieve reliable findings. By adjusting the time step size appropriately throughout a number of time steps, the simulations were conducted with the flow time fluctuation. After several iterations, the time step was eventually decreased to 0.001 s from an initial significantly larger time step of 1 s. For each time step size, the instant values were noted down. **Table 5** illustrates how performance metrics vary with time step size. It can be observed that after-time step size of 0.05 s, the output parameter almost remained constant. The change in C_p value was 1.5% with a further reduction in time step, therefore it was determined that a time step size of 0.05 s was preferable in order to save computing time. After 1500 cycles, the convergence threshold is shown in **Figure 16** to have been reached.

Figure 17 depicts the moment's fluctuation with flow time. Up to 2 s after the periodic state was reached, a non-periodic behavior was visible. Furthermore, the transient

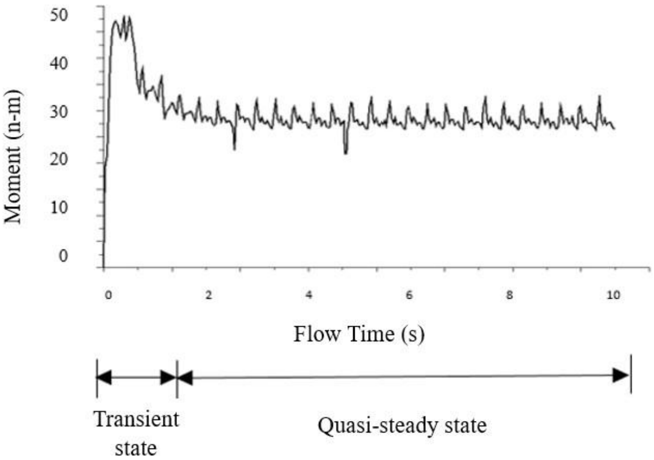

Figure 17. Transient analysis; during the first phase of the rotor's moment generation with flow time, a transient behavior may be seen, followed by a quasi-steady state.

response was taken into account until the rotor reached a quasi-steady state. Once the quasi-steady state was attained, the moment produced by the turbine remained stable.

Figure 18 display the outcomes for static pressure con- tours and velocity vectors. It is clear by looking at the static pressure contour that during each cycle of rotation, the pressure rises in the area of the front exposed to the incoming airflow while falling as it moves towards the downstream side. As can be seen, the velocity vector's intensity is higher in the rotating area and surrounding the rotor blades than it is in the stationary domain. The velocity vectors shift from the upstream side to the downstream side as the airflow moves through the spinning zone. These velocity vectors' various lengths reveal their magnitudes at various locations.

To analyze the flow direction and movement of flow particles closely around the blades and in the domain, velocity vectors were captured. **Figure 19** shows the flow particles' velocity variations and their direction while moving around the turbine blades. The length of vectors shows the magnitude of velocity variation around the blades. The flow particles can be visualized by the direction of vectors. Moreover, to analyze the variation of velocity magnitude, planes were created along the y and z-axis.

3.2.SAVONIUS ROTOR TURBINES

These turbines are drag-based turbines, and the transverse

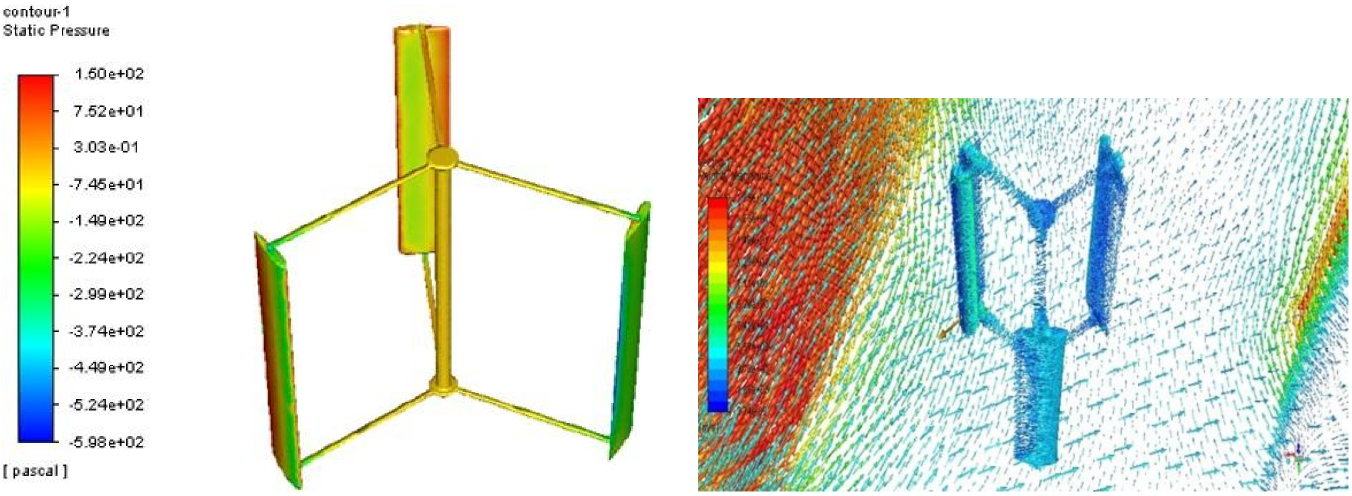

(a) (b)

Figure 18. Contours of (a) static pressure and (b) velocity vectors around the turbine blades. The magnitude of pressure can be seen more at the faces interacting with the incoming airflow.

airflows, along with individual vane and mutual connection of the two sections of the rotor, allow for some integrated rotor performance enhancement. Unlike all drag gears, it has a small operational TSR [55]. This makes it less appropriate for power production than a turbine with higher tip speeds since a higher shaft speed is usually chosen to minimize the step-up ratio condition of the gear- box coupling a rotor to an electrical generator. The most attractive advantages of the Savonius design are simple, economical to construct, low noise and angular rate when in operation, receiving wind from any direction, and can survive in extreme weather situations without momentous damage [56]. Besides, there are numerous variations of this design with respect to blade configuration that affect the performance of the turbine. Several new types of the Savonius turbines have been developed in the last few decades including models with short-span, spiral blades mounted on the wide rotor hub. In these turbines, the resultant airfoil load coincides with the confined flow direction and the same is used to provide rotation. These turbines are available in semi-circular scoops of two or three blades rotor configuration or a cup-shaped hollow cylinder attached with a central rotating shaft [32,57]. The drag force produced during rotation is responsible for torque generation. The energy consumption of these types of turbines is comparatively low and the rotor face is the same as of swept area in blade structure that results in high power to weight ratio. In general, the safety margins assigned to structures during the design phase are typically maintained at smaller or optimal levels in order to fulfill the growing requirements for energy and material conservation [58]. The applications of these turbines are restricted to small-scale projects; however, the utilization can be enhanced with design modifications. These turbines are very effective at low wind speeds because of their low self-starting torque values. The drag-based design extracts the maximum possible energy from the atmosphere due to the difference of drag experienced by each of the blades at the same time. Drag force difference due to the curvature of blades enables the turbine rotor to spin about its axis. The C_p of these types of turbines is approximately 0.12 to 0.25 and the same can be increased with design modification [59].

To assess the performance metrics, Shah *et al.* [60] created four different types of rotor blades: curved, straight, airfoil, and twisted. A MATLAB program was created, and several simulations were executed. The investigation revealed that the straight blade to be the least effective of all, while the twisted blade design can offer high performance. A calculation of the turbine's economic performance revealed an annual power cost per save ratio of roughly \$847. The values of maximum torque coefficient were obtained as 0.06. The study related to roof-mounted Savonius VAWT to install on the house roof was carried out by Dunn *et al.* [57]. Various

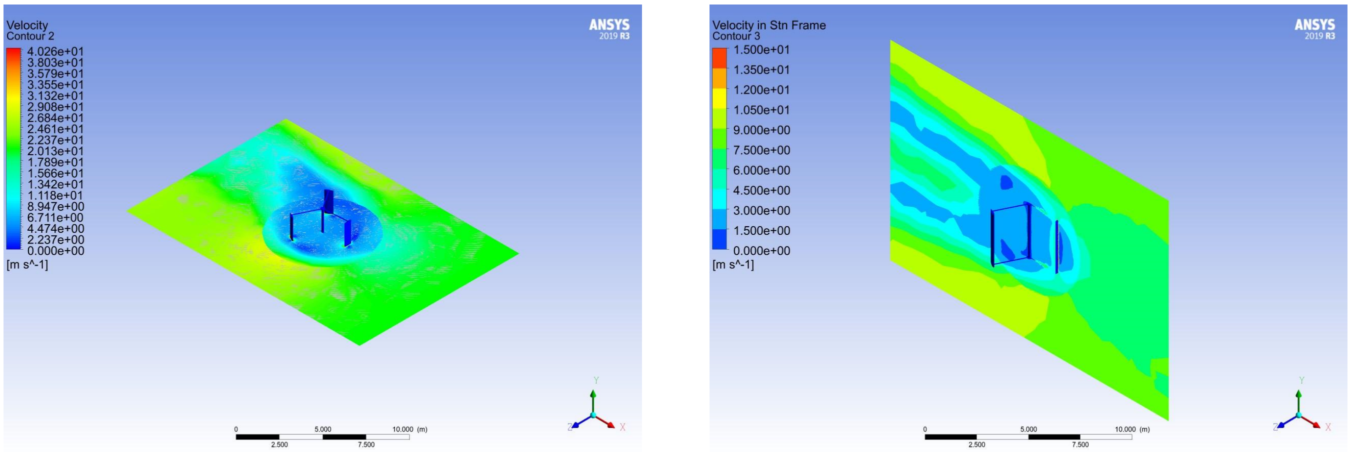

(a) (b)

Figure 19. Distribution of velocity on planes along y and z-axis (a) y = 0.15 m (b) z = 0

turbine blades were studied to maximize the shrouded turbine efficiency. The existing wind data were also analyzed using a wind simulation program. A scaled-down model was tested in a closed-circuit wind tunnel. Turbine rotational speed was measured with the help of an rpm meter. Variation of output power values over a range of wind speed was measured during the study. This project was primarily based on an experimental study. Turbine blades were designed by using S1223 airfoil. According to the analysis conducted both with and without an enclosure, the turbine housed within the enclosure exhibited approximately 73% more power.

The corresponding C_p were determined to be 0.102, 0.237, and 0.222 for the split Savonius turbine without an enclosure, with a 900 enclosure, and for the four-bladed turbine with a 900 enclosure, respectively. In the present study, to compare the flow parameters with the H-Rotor Darrieus turbine, three-dimensional geometry of Savonius wind turbine was developed using ANSYS design modeler as shown in **Figure 20**. Geometric parameters were adopted from an experimental study performed by Kavade *et al.* [49]. The details of the geometric parameters of the Savonius wind turbine are given in **Table 6**.

Table 6. Geometric parameters of the Savonius wind turbine

S No.	Parameter	Value	Unit
1	Blade arc angle	130	deg
2	Blade diameter	0.380	m
3	Blade thickness	0.005	m
4	Rotor height	0.600	m
5	Central shaft diameter	0.040	m
6	Rotor diameter	0.600	m

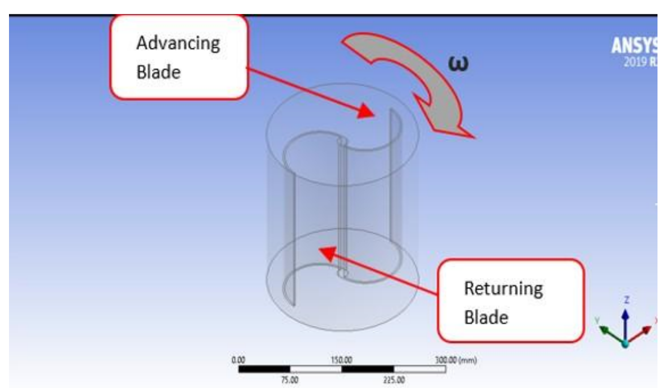

Figure 20. CAD model of Savonius wind turbine

After the generation of geometry, a non-uniform enclosure around the rotor was developed to analyze the flow in the domain. The domain was sized properly upstream, downstream and spanwise on either side of the turbine. The turbine was placed at a hub height of five times the diameter of the blades. Unstructured meshing was performed in the ANSYS meshing module using an unstructured triangular mesh. A coarse mesh element was selected for the outer domain and relatively fine mesh was adapted for the elements near the rotor blades. The mesh size was determined through a grid independence test, following a similar approach to the one used for the H-Rotor Darrieus turbine case. The results of the test, presented in **Table 7**, demonstrate the variation of the C_p with different grid refinement levels. Once the refinement level reaches 2, the C_p value remains constant, indicating that the grid size is now independent and further refinement does not significantly impact the results. The mesh generated around the rotor blades and the outer domain is shown in **Figure 21**.

Table 7. Grid independence test data for Savonius turbine

Refinement level	Elements (Mil)	C_p
Coarse mesh	0.72	0.154
1	1.77	0.192
2	2.67	0.210
3	4.12	0.211
4	6.09	0.210

After creating the mesh within the designated domain, a flow analysis was conducted using the Fluent module. The model was then subjected to transient simulations until it achieved a steady state. The results are also influenced by the time step size; hence, the time step was chosen based on a time step independence study. **Table 8** displays the variation of C_p with different time step sizes. The analysis demonstrated that there were no significant quantitative changes observed for time steps below 0.05 s. Consequently, a time step of 0.05 s was selected for further analysis.

The exit wall was designated as a pressure outlet, while the entrance was designated as a velocity inlet. The domain's remaining four sides were designated as symmetry boundary walls. In order to perform the CFD analysis, a k–ϵ turbulence model was used. For one set of boundary conditions, inlet velocity was selected as 5 m/s with outlet pressure zero-gauge pressures. The solution was initiated using hybrid initialization and results were captured with variation from the inlet and about 1000 time steps by the selection of appropriate step size. Post-processing results were obtained for velocity contours and velocity streamlines. **Figure 22** shows the velocity streamlines at various time intervals along with the change in velocity field around the rotor. The velocity variations around the turbine blades and flow separation along with the wake region can easily be visualized to capture the flow parameters.

Table 8. Time step independence data for Savonius turbine

S. No	Time step (s)	Power coefficient (Cp)
1	1	0.251
2	0.5	0.234
3	0.1	0.227
4	0.05	0.210
5	0.01	0.210
6	0.005	0.211
7	0.001	0.212

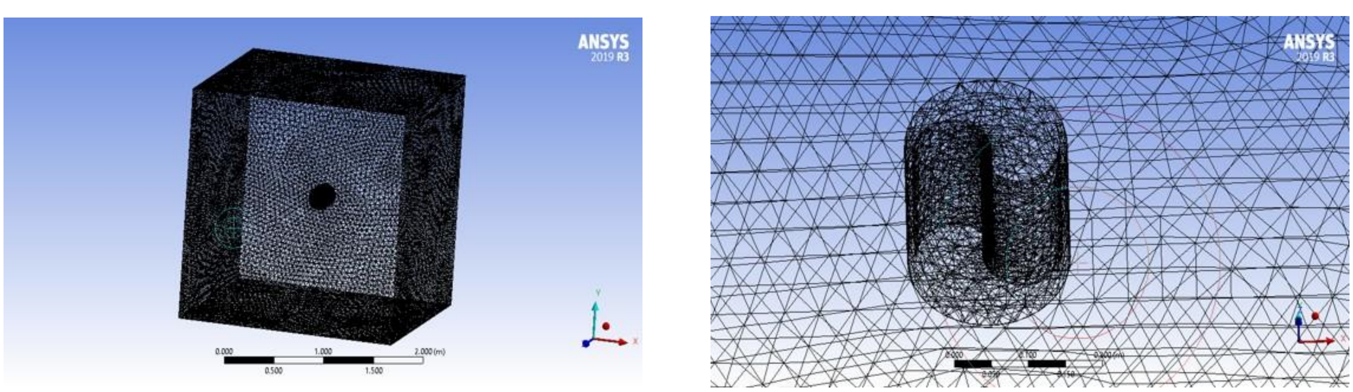

(a) (b)

Figure 21. Mesh generated in ANSYS mesh module (a) complete domain, (b) rotor surface.

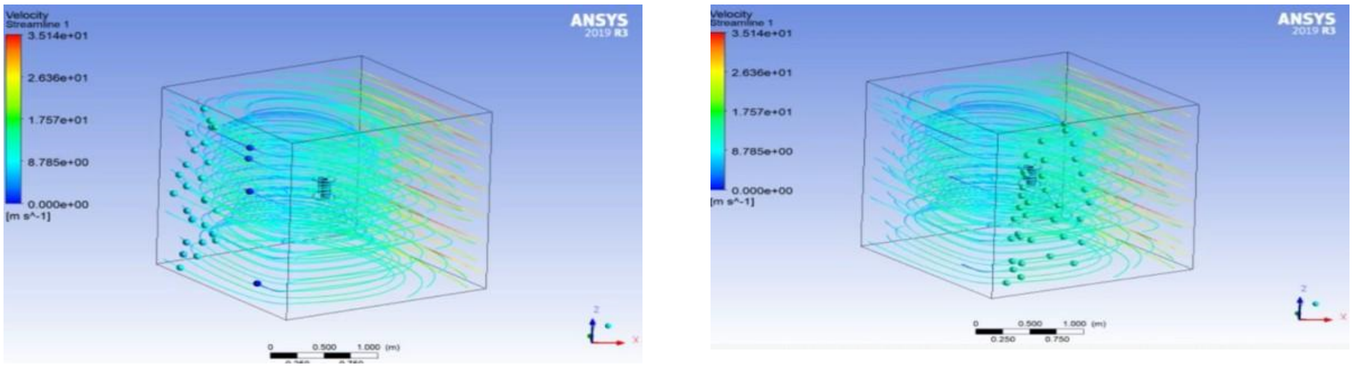

(a) (b)

Figure 22. Velocity streamlines at different time intervals (a) 1 s, (b) 2 s.

3.3.RESULTS AND DISCUSSION

Parametric studies were performed for the above-mentioned cases of CFD analysis. Cases were run under various wind speeds and TSR settings. Initially, for the 2D case, the large circular domain velocity was kept at 60 rpm and small blade rotation was selected half with respect to the large domain. Simulations were run for inlet velocity variation up to 10–12 m/s. Results were obtained for each of the predefined set of flow variables. **Figure 23** illustrates the variation of output power with wind speed for two types of wind turbines: Savonius and H-Rotor Darrieus. It is evident from the plot that Savonius turbine starts generating power at 2 m/s, while the H-Rotor Darrieus requires a slightly higher wind speed of 3.1 m/s to begin operation. Moreover, the maximum rated power of the H-Rotor Darrieus turbine is 30 watts, which is significantly higher than the Savonius turbine's maximum rated power of 5 watts. This makes the H-Rotor Darrieus turbine more suitable for applications where higher power output is required.

At low wind speeds, the drag-based design of the Savonius turbine allows it to extract the maximum possible energy. This is achieved by exploiting the different drag forces experienced by each of the turbine's blades, which enables the rotor to spin about its axis and generate power. In contrast, the H-Rotor Darrieus turbine operates on lift-based principles, and while it may not be as efficient at low wind speeds, it is capable of producing more energy than the Savonius turbine at higher wind speeds.

To validate the obtained results, a comparison was

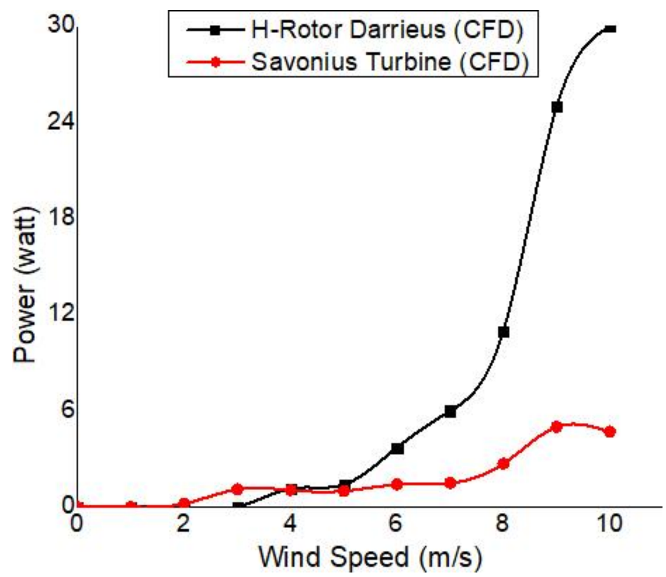

Figure 23. Comparison of output power results obtained from CFD, H-Rotor Darrieus started producing power after Savonius, a significant difference can be seen at 3 and 9 m/s.

carried out with the experimental testing performed by Kavade *et al.* [49]. **Figure 24** presents a comprehensive comparative analysis of the output power versus wind speed for two types of turbines. The data obtained from the experiments closely align with the results shown in the figure for both turbine designs. At their respective rated power points, the absolute difference between the experimental and CFD values is 1.3 watts for the Savonius turbine and 4.5 watts for the H-Rotor Darrieus turbine. These small absolute differences are indicative of the accuracy and reliability of the simulations. The proximity between the experimental and CFD data points reinforces the validity of the models employed in predicting the turbines performance under different wind speeds. The

Savonius turbine exhibits a slight deviation of 1.3 watts at its rated power point, which is well within acceptable tolerances. This finding underscores the effectiveness of the drag-based design of the Savonius turbine in extracting energy from low wind speeds and converting it into usable power. Similarly, the H-Rotor Darrieus turbine demonstrates a difference of 4.5 watts at its rated power, which, considering the higher power output of this lift-based turbine, is also deemed to be within an acceptable range of accuracy. The lift-based design allows the H-Rotor Darrieus turbine to harness greater amounts of wind energy, making it an advantageous choice for applications where higher power generation is required. The comparison of the findings demonstrates that there is a lot of energy in the wind. The efficiency of the wind turbine and its de- sign characteristics have a significant impact on the output power generated by the wind.

The power coefficient (C_p) is an important parameter to determine the performance characteristics of the wind turbine. The C_p value represents the ratio of the actual power extracted by the turbine to the available power in the wind, and a higher C_p value implies better energy conversion. The larger is the turbine efficiency or C_p, the more power can be extracted from the wind. **Figure 25** presents a comparative analysis of the power coefficient (C_p) versus wind speed for both H-Rotor Darrieus and Savonius turbines. In particular, **Figure 25a** focuses on the C_p values obtained through CFD simulations for two configurations of the H-Rotor Darrieus turbine. For the 2D CFD simulation of the H-Rotor Darrieus turbine, the maximum C_p value of 0.37 is achieved at a wind speed of 8 m/s. This indicates the optimal efficiency of the turbine at that specific wind speed when operating under two- dimensional flow conditions. In this case, the maximum C_p value achieved is 0.32, also occurring at a wind speed of 8 m/s. The slight difference in C_p values between the 2D and 3D designs can be attributed to the three-dimensional flow effects that come into play in the 3D CFD model. De- spite the decrease in C_p compared to the 2D simulation, a C_p of 0.32 is still indicative of a reasonably efficient energy conversion for the H-Rotor Darrieus turbine under 3D flow conditions.

The observed discrepancies between the CFD results and experimental values for the H-Rotor Darrieus turbine, particularly at high wind speeds, can be attributed to the complex aerodynamics involved in this turbine design. The intricate interaction between the rotating blades and the incoming wind creates challenging flow patterns, including regions of separated flow, vortex shedding, and blade stall, which are more pronounced at high wind speeds. Additionally, uncertainties arise from the boundary conditions set in the CFD simulations, which may not fully match the real-world experimental setup. The choice of turbulence model and its settings in the

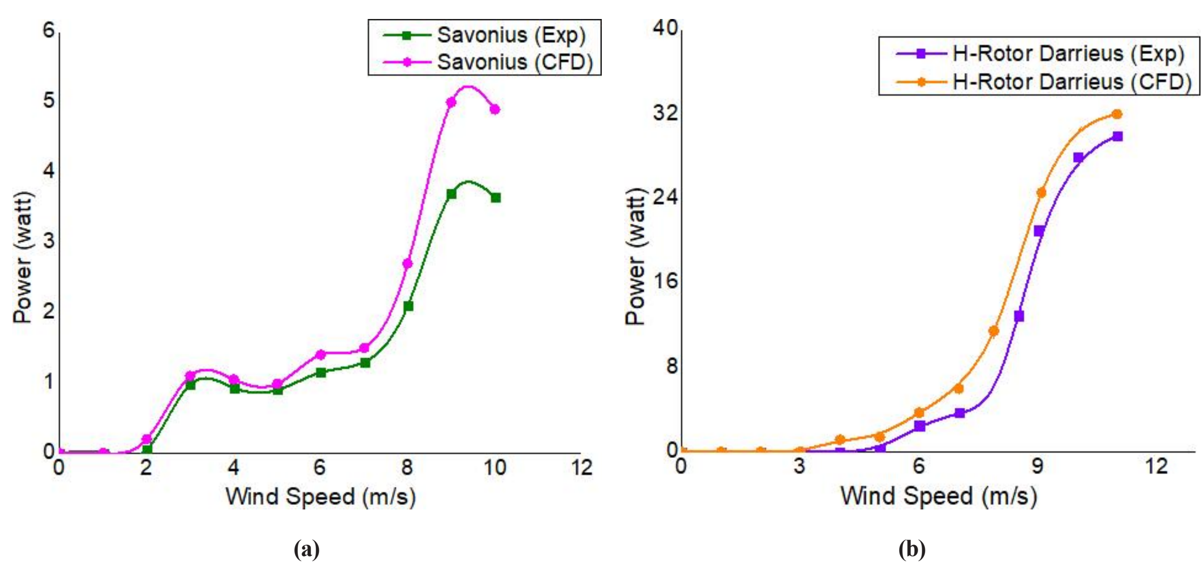

Figure 24. Variation of output power for (a) Savonius turbine, (b) H-Rotor Darrieus; the obtained CFD results are quite close with the experimental results in both the cases and the overall output power of H-Rotor Darrieus is more after cut-in speed.

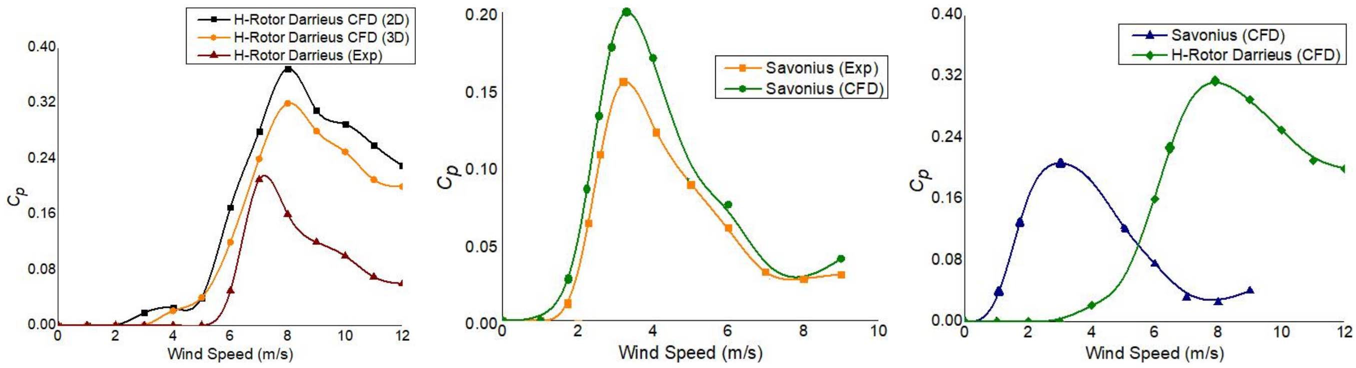

(a) (b) (c)

Figure 25. Analysis of power coefficient (Cp) versus wind speed (a) H-Rotor Darrieus (CFD and Experimental) (b) Savonius turbine (CFD and Experimental) (c) H-Rotor Darrieus (CFD) versus Savonius turbine (CFD). The obtained results are quite close with the experimental results in both the cases. Savonius started producing power at low wind speed and the maximum Cp of H-Rotor Darrieus is more at higher wind speed ranges in both analysis techniques.

CFD simulations can also influence the accuracy of the results, especially in areas of complex flow. Furthermore, geometric simplifications in the CFD model might overlook certain real- world complexities, such as blade surface roughness and structural support effects. On the experimental side, the measurements are susceptible to uncertainties, including measurement errors, calibration issues, and other limitations inherent in the experimental setup. The probable cause of the difference in both experimental and numerical techniques may also be attributed to manufacturing flaws, frictional losses, numerical assumptions, and environmental conditions. Addressing these challenges requires a meticulous investigation of each factor's impact and a more robust validation process for both CFD and experimental testing to achieve improved agreement between simulation and real-world performance.

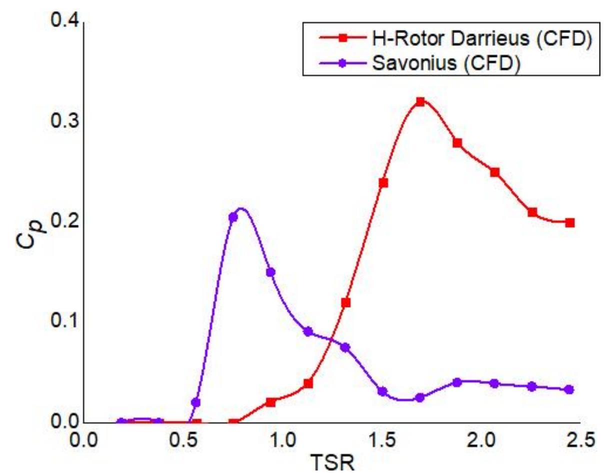

Figure 26. Variation of power coefficient (Cp) with TSR. Savonius turbine shows self-starting capability at low TSR (0.5); however, the maximum Cp value of H-Rotor Darrieus is more at TSR of 1.69.

The variation of the C_p for both types of turbines with TSR is shown in **Figure 26**. The analysis indicates that the H-Rotor Darrieus turbine reaches its peak power coefficient (C_p) at approximately 8 m/s wind speed. Using this value as the design speed, C_p values were obtained for various TSRs. Initially, when the wind turbine starts rotating, the rotational velocity is zero, resulting in no output power. As the rotation speed increases, the turbine begins extracting power from the wind, reaching maximum rotational velocity and maximum power extraction. Beyond this point, a decline in power coefficient can be observed. In this study, the maximum C_p for the H-Rotor Darrieus turbine was found to be 0.32 at a TSR of 1.69. Similarly, for the Savonius turbine, the maximum C_p was determined to be 0.21 at a TSR of 0.75. These values represent the efficiency of each turbine type in converting wind energy into usable power at their respective TSRs. The analysis also provides a visual understanding of how the power coefficient changes as the TSR is varied, and it reveals the optimal TSR for maximum power extraction in each turbine design. These findings are crucial for turbine design and performance optimization, as selecting the appropriate TSR is essential to achieve the best possible energy conversion efficiency. Additionally, the comparison between the H-Rotor Darrieus and Savonius turbines in terms of their values sheds light on their relative performance under different

TSR conditions.

4.CONCLUSION

Wind energy remains a prime source of green energy these days as the available energy resources are continuously depleting. Both VAWTs and HAWTs are used for extracting the electrical power from the wind, however, to get the maximum output power, design parameters of the wind turbine are to be chosen carefully. In comparison to HAWTs, VAWTs have a number of benefits, including omnidirectional operation, simple installation and maintenance, generator location, independence from the yaw mechanism, ability to operate in turbulent flow zones, rooftops, and gusty winds, cheap cost, high working wind speed limitations, minimal noise profile, and high fatigue life. The simplest form of lift force-based VAWT with two or more blades is the H-Rotor Darrieus turbine. This blade arrangement can have blades with constant or variable pitch. In addition to the independent vanes and inter- connection between the two rotor parts, Savonius turbines are drag force-driven turbines that incorporate certain enhancements to improve their performance. While these turbines exhibit strong starting capabilities, their power coefficient is relatively low compared to other VAWTs, typ- ically ranging from 0.12 to 0.25. In this research study, two types of VAWTs, namely H-Rotor Darrieus and Savonius, were analyzed using the ANSYS-Fluent commercial package. Blade design and the number of blades play a critical role in performance and energy extraction from the tur- bine. The sliding mesh technique was used which is very efficient and leads to a good approximation of flow-field analysis. A transient flow analysis using the second-order k-ϵ turbulence model for both types of turbines has been carried out. After analyzing the results, it was concluded that the C_p of the Savonius turbine with two blades configuration is less than H-Rotor Darrieus. Savonius turbine showed good starting capability as described in the literature, however, its overall performance is less than H-Rotor

Darrieus turbine. The performance of the Darrieus turbine is better at higher wind speeds. The maximum values of C_p for H-Rotor Darrieus and Savonius were obtained as 0.32 and 0.21 at TSR of 1.69 and 0.75, respectively. The obtained results are quite close to the experimental data. The self-starting problem can be minimized by us- ing cambered airfoil; however, overall performance may be degraded. The C_p of a Savonius wind turbine with a two-blade configuration rises with TSR; however, when the number of blades is increased, the C_p value decreases due to the increased drag caused by the additional blades. This results in a higher reverse torque and a reduction in the net torque applied to the blades. Hybrid VAWT combines Darrieus and Savonius VAWT to address issues with efficiency and self-starting. This design is regarded as an effective way to draw electricity from challenging urban topography in urban regions.

The VAWTs can demonstrate effective performance in environments characterized by turbulent flow. However, it is important to note that VAWTs generally exhibit lower overall efficiency compared to traditional HAWTs. As the potential for VAWT expansion is considered, it becomes crucial to explore approaches that can enhance the power coefficient and self-starting capabilities, particularly at low wind speeds. One possible avenue for improvement lies in the optimization of design parameters. In this regard, the design, analysis, and prototyping of a hybrid lift-drag type VAWT can offer a unique technical solution to address the limitations of conventional systems. By incorporating both lift and drag-based turbine features, a hybrid VAWT can leverage the advantages of both approaches and potentially overcome the drawbacks associated with each individual type.

The present research on the aerodynamic performance of VAWTs using computational techniques has implications for various stakeholders in the renewable energy industry. Wind turbine manufacturers can optimize their designs for improved efficiency and cost-effectiveness. Renewable energy researchers can use the findings as a foundation for further investigations. Engineers and designers can make informed decisions during the design process, while policy makers and governments can utilize its insights for evidence-based policy decisions and investments in wind energy. Sustainable energy enthusiasts can find inspiration for adopting renewable energy technologies. Overall, this study contributes to advancing wind turbine technology and promoting a greener and more sustainable energy landscape.

DISCLOSURE STATEMENT

The authors declare that no conflict of interest.

REFERENCES

[1] Saidur R, Rahim NA, Islam RM, et al., 2011, Environmental Impact of Wind Energy. Renewable and Sustainable Energy Reviews, 15(5): 2423–2430.

[2] Islam MR, Mekhilef S, Saidur R, 2013, Progress and Recent Trends of Wind Energy. Technology. Renewable and Sustainable Energy Reviews. 21: 456–468.

[3] Kaldellis JK, Zafirakis D, 2011, The Wind Energy (R) Evolution: A Short Review of a Long History. Renewable Energy, 36(7): 1887–1901.

[4] Ahmad M, Shahzad A, Qadri MNM, 2022, An Overview of Aerodynamic Performance Analysis of Vertical Axis Wind Turbines. Energy & Environment, 2022: 0958305X221121281.

[5] Ahmad M, Shahzad A, Akram F, et al., 2022, Design Optimization of Double-Darrieus Hybrid Vertical Axis Wind Turbine. Ocean Engineering, 254: 111171.

[6] Keerthana M, Sriramkrishnan M, Velayutham T, et al., 2012, Aerodynamic Analysis of a Small Horizontal Axis Wind Turbine Using CFD. Journal of Wind and Engineering, 9(2): 14–28.

[7] Aman M, Jasmon G, Ghufran A., et al., 2013, Investigating Possible Wind Energy Potential to Meet the Power Shortage in Karachi. Renewable and Sustainable Energy Reviews, 18: 528–542.

[8] Eriksson S, Bernhoff H, Leijon M, 2008, Evaluation of Different Turbine Concepts for Wind Power. Renewable and Sustainable Energy Reviews, 12(5): 1419–1434.

[9] Nikam D, Kherde S, 2015, Literature Review on Design and Development of Vertical Axis Wind Turbine Blade. Proceedings of the National Conference on Emerging Research Trends in Engineering and Technology (NCERT), 156–161.

[10] Ahmad M, Shahzad A, Akram F, et al., 2022, Determination of Efficient Configurations of Vertical Axis Wind Turbine Using Design of Experiments. Proceedings of the Institution of Mechanical Engineers, 1558–1581.

[11] Zhao Z, Wang D, Wang T, et al., 2022, A Review: Approaches for Aerodynamic Performance Improvement of Lift-Type Vertical Axis Wind Turbine. Sustainable Energy Technologies and Assessments, 49: 101789.

[12] Ahmad M, Shahzad A, Shah SIA, 2023, Experimental Investigation and Analysis of Proposed Hybrid Vertical Axis Wind Turbine Design. Energy & Environment, 2023: 0958305X231181675.

[13] Aho J, Buckspan A, Laks J, et al., 2012, A Tutorial of Wind Turbine Control for Supporting Grid Frequency Through Active Power Control. Proceedings of American Control Conference (ACC), 3120–3131.

[14] Han Z, Chen H, Chen Y, et al., 2013, Aerodynamic Performance Optimization of Vertical Axis Wind Turbine with Straight Blades Based on Synergic Control of Pitch and Flap, Sustainable Energy Technologies and Assessments, 57: 103250.

[15] Saad MMM, Asmuin N, 2014, Comparison of Horizontal Axis Wind Turbines and Vertical Axis Wind Turbines. IOSR Journal of Engineering (IOSRJEN), 4(08): 27–30.

[16] Paulides J, Encica L, Jansen J, et al., 2009, Small-Scale Urban Venturi Wind Turbine: Direct-Drive Generator. Proceedings of 2009 IEEE International Electric Machines and Drives Conference, 1368–1373.

[17] Tang H, Lam KM, Shum KM, et al., 2019, Wake Effect of a Horizontal Axis Wind Turbine on the Performance of a Downstream Turbine. Energies, 12(12): 2395.

[18] Peacock A, Jenkins D, Ahadzi M, et al., 2008, Micro wind turbines in the UK domestic sector, Energy and buildings, 40(7): 1324–1333.

[19] Ishugah T, Li Y, Wang R, et al., 2014, Advances in Wind Energy Resource Exploitation in Urban Environment: A Review. Renewable and Sustainable Energy Reviews, 37: 613–626.

[20] Winslow AR, 2017, Urban Wind Generation: Comparing Horizontal and Vertical Axis Wind Turbines at Clark University in Worcester, Massachusetts, master's paper, Clark University.

[21] Goldberg SB, 1995, Vertical-Axis Wind Turbine with a Twisted Blade Configuration, US Patent, 5,405,246 (April 11, 1995).

[22] Toja-Silva F, Colmenar-Santos A, Castro-Gil M, 2013, Urban Wind Energy Exploitation Systems: Behaviour Under Multidirectional Flow Conditions — Opportunities and Challenges. Renewable and Sustainable Energy Reviews, 24: 364–378.

[23] Li Y, Yang S, Feng F, et al., 2023, A Review on Numerical Simulation Based on CFD Technology of Aerodynamic Characteristics of Straight-Bladed Vertical Axis Wind Turbines. Energy Reports, 9: 4360–4379.

[24] Kim SH, Suh K, 2020, Experimental and Numerical Investigation on Power Characteristics of 300 W Class Horizontal Axis Wind Turbine with Wave Winding Type AFPM Generator. International Journal of Precision Engineering and Manufacturing- Green Technology, 7(4): 837–848.

[25] Bhutta MMA, Hayat N, Farooq AU, et al., 2012, Vertical Axis Wind Turbine – A Review of Various Configurations and Design Techniques. Renewable and Sustainable Energy Reviews, 16(4): 1926–1939.

[26] Shahariar GH, Hasan MR, 2014, Design & Construction of a Vertical Axis Wind Turbine, Proceedings of the 2014 9th International Forum on Strategic Technology (IFOST), 326–329.

[27] Tjiu W, Marnoto T, Mat S, M. H. Ruslan, K. Sopian, Darrieus Vertical Axis Wind Turbine for Power Generation I: Assessment of Darrieus VAWT Configurations. Renewable Energy, 75: 50–67.

[28] Mohammed AA, Ouakad HM, Sahin AM, et al., 2019, Vertical Axis Wind Turbine Aerodynamics: Summary and Review of Momentum Models. Journal of Energy Resources Technology 141(5): 050801.

[29] Mertens S, van Kuik G, van Bussel G, 2003, Performance of an H-Darrieus in the Skewed Flow on a Roof. J. Sol. Energy Eng., 125(4): 433–440.

[30] Howell R, Qin N, Edwards J, et al., 2010, Wind Tunnel and Numerical Study of a Small Vertical Axis Wind Turbine. Renewable Energy, 35(2): 412–422.

[31] Gorelov D, Krivospitsky V, 2008, Prospects for Development of Wind Turbines with Orthogonal Rotor. Thermophysics and Aeromechanics, 15: 153–157.

[32] Islam M, Ting DSK, Fartaj A, 2008, Aerodynamic Models for Darrieus-Type Straight-Bladed Vertical Axis Wind Turbines. Renewable and Sustainable Energy Reviews, 12(4): 1087–1109.

[33] Hussen MS, Rambabu K, Ramji M, et al., 2015, Design and Analysis of Vertical Axis Wind Turbine Rotors. International Journal on Recent Technologies in Mechanical and Electrical Engineering (IJRMEE), 2(9): 54–62.

[34] Das N, Sohail A, Doley R, 2022, Computational Fluid Dynamics Analysis of Wind Turbine Blades at Various Angles of Attack, in Advances in Smart Energy Systems, Springer, 175–184.

[35] Alaimo A, Esposito A, Messineo A, et al.,2015, 3D CFD Analysis of a Vertical Axis Wind Turbine. Energies, 8(4): 3013–3033.

[36] Sabaeifard P, Razzaghi H, Forouzandeh A, 2012, Determination of Vertical Axis Wind Turbines Optimal Configuration Through CFD Simulations, in International Conference on Future Environment and Energy, 28: 109–113.

[37] Airfoil Tools, n.d., viewed July 28, 2023, http://airfoiltools.com/

[38] Cao H, 2011, Aerodynamics Analysis of Small Horizontal Axis Wind Turbine Blades by Using 2D and 3D CFD Modelling, thesis, University of central Lancashire.

[39] Sargsyan A, 2010, Simulation and Modeling of Flow Field Around a Horizontal Axis Wind Turbine (HAWT) Using RANS Method, Florida Atlantic University.

[40] Temam R, 2001, Navier-Stokes Equations: Theory and Numerical Analysis, Volume 343, AMS Chelsea Publishing, New York.

[41] Galdi G, 2011, An Introduction to the Mathematical Theory of the Navier-Stokes Equations: Steady-State Problems, Springer Science & Business Media, Berlin/Heidelberg.

[42] Parra T, Vega C, Gallegos A, et al., 2015, Design of h-Darrieus Vertical Axis Wind Turbine, in EPJ Web of Conferences, 92: 2058.

[43] Davis CJ, 2012, Computational Modeling of Wind Turbine Wake interactions, thesis, Colorado State University.

[44] Ghosh A, Biswas A, Sharma K, et al., 2015, Computational Analysis of Flow Physics of a Combined Three Bladed Darrieus Savonius Wind Rotor. Journal of the Energy Institute 88 (4) () 425–437.

[45] Gupta R, Sharma K, 2012, Flow Physics of a Combined Darrieus-Savonius Rotor Using Computational Fluid Dynamics (cfd), International Research Journal of Engineering Science, Technology and Innovation. 1(1): 1–13.

[46] Mohamed M, 2012, Performance Investigation of h-Rotor Darrieus Turbine with New Airfoil Shapes, Energy 47(1): 522–530.

[47] Hosseini A, Goudarzi N, 2019, Design and CFD Study of a Hybrid Vertical-Axis Wind Turbine by Employing a Combined Bach-Type and h-Darrieus Rotor Systems, Energy Conversion and management 189: 49–59.

[48] Cooper P, 2010, Development and Analysis of Vertical-Axis Wind Turbines, Wind Power Generation and Wind Turbine Design, 277.

[49] Kavade RK, Ghanegaonkar PM, 2017, Design and Analysis of Vertical Axis Wind Turbine for Household Application, Journal of Clean Energy Technologies, 5(5): 353–358.

[50] Lanzafame R, Mauro S, Messina M, 2014, 2D CFD modeling of h- darrieus wind turbines using a transition turbulence model, En- ergy Procedia 45: 131–140.

[51] Langtry R, Gola J, Menter F, 2006, Predicting 2D airfoil and 3D Wind Turbine Rotor Performance Using a Transition Model for General CFD Codes. Proceedings of 44th AIAA Aerospace Sciences Meeting and Exhibit, 395.

[52] Didane DH, Rosly N, Zulkafli MF, et al., Numerical Investigation of a Novel Contra-Rotating Vertical Axis Wind Turbine. Sustainable Energy Technologies and Assessments. 31: 43–53.

[53] Ahmad M, Hussain ZL, Shah SIA, et al., 2021, Estimation of Stability Parameters for Wide Body Aircraft Using Computational Techniques. Applied Sciences 11(5): 2087.

[54] Wilcox DC, 1998, Turbulence Modeling for CFD, Volume 2, DCW Industries La Canada, California.

[55] Kim S, Cheong C, 2015, Development of Low-Noise Drag-Type Vertical Wind Turbines. Renewable Energy, 79: 199–208.

[56] Bajuri MNA, Didane DH, Boukhari MI, et al., 2022, Computational Fluid Dynamics (CFD) Analysis of Different Sizes of Savonius Rotor Wind Turbine. Journal of Advanced Research in Applied Mechanics, 94(1): 7–12.

[57] Deisadze L, Digeser D, Dunn C, et al., 2013, Vertical Axis Wind Turbine Evaluation and Design, Worcester Polytechnic Institute.

[58] Khan AA, Ahmad M, Ashraf M, 2016, Residual Life Estimation of an Attach Angle for a Cargo Aircraft. Journal of Failure Analysis and Prevention, 16: 1126–1133.

[59] Mohamed M, Janiga G, Pap E, et al., 2011, Optimal Blade Shape of a Modified Savonius Turbine Using an Obstacle Shielding the Returning Blade. Energy Conversion and Management, 52(1): 236–242.

[60] Shah SR, Kumar R, Raahemifar K, et al., 2018, Design, Modeling and Economic Performance of a Vertical Axis Wind Turbine. Energy Reports. 4: 619–623.

Muhammad Ahmad holds a Master's degree in Aerospace Engineering and specializes in Computational Fluid Dynamics (CFD), Aerodynamics, Design Optimization, and Wind Energy Harvesting. With an academic background and expertise in these areas, he has contributed significantly to research and development efforts in the aerospace and renewable energy sectors. His passion for advancing aerospace engineering and wind energy technologies drives him to address complex challenges and strive for sustainable and efficient solutions.

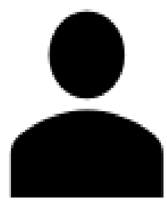

Iram Rehman holds a Master's degree in English Literature and stands as a dedicated scholar and practitioner in the field. With a keen eye for detail and a passion for linguistic precision, Iram has seamlessly ventured into the realm of editing, ensuring that written works achieve a pinnacle of clarity and coherence. Her role as a perceptive reviewer has contributed valuable insights to the literary discourse, while her academic journey reflects a commitment to scholarly excellence. With a deep-rooted appreciation for literature, Iram's multifaceted contributions continue to resonate within the academic and literary communities.

Publisher's note

Art and Design Publishing remains neutral with regard to jurisdictional claims in published maps and institutional affiliations.